



Article

Porcine Enteric Coronavirus PEDV Induces the ROS-ATM and Caspase7-CAD- γ H2AX Signaling Pathways to Foster Its Replication

Xin Ming^{1,†}, Huan Chen^{1,†}, Ying Yang¹, Pu Zhao¹, Liumei Sun^{1,2}, Caisheng Zhang¹, Hyun-Jin Shin³, Jeong-Soo Lee⁴, Yong-Sam Jung¹ and Yingjuan Qian^{1,5,*}

¹ MOE Joint International Research Laboratory of Animal Health and Food Safety, Jiangsu Foreign Expert Workshop, College of Veterinary Medicine, Nanjing Agricultural University, Nanjing 210095, China

² Jiangsu Key Laboratory of Sericultural Biology and Biotechnology, School of Biotechnology, Jiangsu University of Science and Technology, Zhenjiang 212100, China

³ College of Veterinary Medicine, Chungnam National University, Daejeon 305-764, Korea

⁴ Department of Electrical Engineering, Pohang University of Science and Technology (POSTECH), Pohang 37673, Korea

⁵ Jiangsu Key Laboratory for High-Tech Research and Development of Veterinary Biopharmaceuticals, Jiangsu Agri-Animal Husbandry Vocational College, Taizhou 225300, China

* Correspondence: yqian@njau.edu.cn; Tel.: +86-25-8439-9102

† These authors contributed equally to this work.



Citation: Ming, X.; Chen, H.; Yang, Y.; Zhao, P.; Sun, L.; Zhang, C.; Shin, H.-J.; Lee, J.-S.; Jung, Y.-S.; Qian, Y. Porcine Enteric Coronavirus PEDV Induces the ROS-ATM and Caspase7-CAD- γ H2AX Signaling Pathways to Foster Its Replication. *Viruses* **2022**, *14*, 1782. <https://doi.org/10.3390/v14081782>

Academic Editor: Tohru Suzuki

Received: 29 July 2022

Accepted: 12 August 2022

Published: 15 August 2022

Publisher's Note: MDPI stays neutral with regard to jurisdictional claims in published maps and institutional affiliations.



Copyright: © 2022 by the authors. Licensee MDPI, Basel, Switzerland. This article is an open access article distributed under the terms and conditions of the Creative Commons Attribution (CC BY) license (<https://creativecommons.org/licenses/by/4.0/>).

Abstract: DNA damage response (DDR) is an evolutionarily conserved mechanism by which eukaryotic cells sense DNA lesions caused by intrinsic and extrinsic stimuli, including virus infection. Although interactions between DNA viruses and DDR have been extensively studied, how RNA viruses, especially coronaviruses, regulate DDR remains unknown. A previous study showed that the porcine epidemic diarrhea virus (PEDV), a member of the genus *Alphacoronavirus* in the *Coronaviridae* family, induces DDR in infected cells. However, the underlying mechanism was unclear. This study showed that PEDV activates the ATM-Chk2 signaling, while inhibition of ATM or Chk2 dampens the early stage of PEDV infection. Additionally, we found that PEDV-activated ATM signaling correlates with intracellular ROS production. Interestingly, we showed that, unlike the typical γ H2AX foci, PEDV infection leads to a unique γ H2AX staining pattern, including phase I (nuclear ring staining), II (pan-nuclear staining), and III (co-staining with apoptotic bodies), which highly resembles the apoptosis process. Furthermore, we demonstrated that PEDV-induced H2AX phosphorylation depends on the activation of caspase-7 and caspase-activated DNase (CAD), but not ATM-Chk2. Finally, we showed that the knockdown of H2AX attenuates PEDV replication. Taken together, we conclude that PEDV induces DDR through the ROS-ATM and caspase7-CAD- γ H2AX signaling pathways to foster its early replication.

Keywords: PEDV; ATM; γ H2AX; caspase; DNA damage response

1. Introduction

Viruses have evolved sophisticated tactics to optimize the intracellular environment by hijacking cellular signaling pathways for their replication. The DNA damage response (DDR) is a complex three-tiered signaling cascade that is mediated by ataxia telangiectasia mutated (ATM), ATM and Rad3 related (ATR), and DNA-dependent protein kinase (DNA-PK), leading to DNA repair, cell cycle arrest, and apoptosis according to the extent of damage [1–4]. As a causative factor in oncogenesis and chronic inflammation, the interplay between DDR and oncogenic viruses has been extensively studied. However, many non-oncogenic RNA viruses can also induce DDR [5]. For example, hepatitis C virus (HCV) infection stimulates the production of Nitric oxide (NO) and Reactive oxygen species (ROS) and subsequently induces DNA damage and genetic abnormalities [6,7]. Infectious

bronchitis virus (IBV), a member of the *Coronaviridae* family, activates the replicative stress and ATR pathway through the interaction between the nsp13 and DNA polymerase δ , leading to the S-phase arrest, which benefits viral replication [8]. A recent study showed that severe acute respiratory syndrome coronavirus 2 (SARS-CoV-2) infection also activates the ATR-Chk1 pathway and induces H2AX phosphorylation [9].

Porcine epidemic diarrhea (PED) is an acute and highly contagious enteric disease characterized by severe watery diarrhea, dehydration, and anorexia in piglets [10]. The causative agent is the porcine epidemic diarrhea virus (PEDV), an enveloped, single-stranded positive-sense RNA virus, which belongs to the family *Coronaviridae*, genus *Alphacoronavirus* [11]. The PEDV genome is approximately 28 kb in size and encodes replicase polyprotein (pp) 1a and pp1ab, which are subsequently cleaved into sixteen non-structural proteins (NSPs), four structural proteins, spike (S), membrane (M), envelope (E), nucleocapsid (N), and one accessory protein ORF3 [12]. In 2013, PED emerged in the United States and rapidly spread across North America and Asia, causing a devastating impact on the global swine industry [13–16]. To unravel its pathogenesis, many researchers endeavor to explore the interaction between PEDV and many important host signaling pathways including autophagy, innate immune response and apoptosis [17–22]. Studies showed that the pathological changes of PEDV infection in vivo were related to the activation of the cellular apoptotic pathway [23–25]. In addition, PEDV infection induces the phosphorylation of Chk2 and H2AX, resulting in cell cycle arrest in the G1/G0 phase. However, the molecular mechanism of PEDV regulating the cellular DDR and the significance of DDR on PEDV replication remain unclear.

In this study, we further investigated the interaction between DDRs and PEDV infection. We showed that PEDV infection strongly activates the ATM-Chk2 signaling pathway in both Vero-E6 and Marc145 cells. Interestingly, we observed a unique γ H2AX staining pattern that differs from the typical DDR foci. In addition, we found that the activation of ATM signaling is associated with the elevated level of cellular ROS, whereas the phosphorylation of H2AX is independent of ATM activity, but associated with caspase and CAD activation. Moreover, inhibition of ATM signaling by a specific inhibitor or siRNA interference largely attenuates PEDV early replication. Consistently, we demonstrated that H2AX plays a positive role in PEDV replication. Taken together, these findings suggest that PEDV infection regulates ATM-Chk2 signaling and H2AX phosphorylation through two independent mechanisms to promote PEDV replication.

2. Materials and Methods

2.1. Cells and Viruses

Vero-E6 and Marc145 cells were cultured in Dulbecco's modified Eagle's medium (DMEM, Gibco) supplemented with 10% fetal bovine serum (Pan-Biotech, Inc. Bavaria, Aidenbach, Germany) at 37 °C with 5% CO₂. Two PEDV strains, CV777, a vaccine strain, and HLJBY (KP403802.1), a virulence-attenuated strain, were used in this study.

2.2. Plasmids and Reagents

ICAD/DFFA/DFF45 (NM_004401.3) was amplified from cDNA prepared with MCF7 cells, and ICAD mutants were amplified from ICAD construct with primers listed in Table 1. PCR fragments were cloned into pcDNA3-Flag using ClonExpress Ultra One Step Cloning Kit (Vazyme Biotech, Inc. Nanjing, China). Hydroxyurea (HU), Apocynin (APO), Acetylcysteine (NAC), Diphenyleneiodonium chloride (DPI), and caspase 3/7 inhibitors Ac-DEVD-CHO, ATM inhibitor KU55933, and ATR inhibitor VE-821 were purchased from Selleck Chemicals Inc. (Houston, TX, USA). Caspase pan-inhibitor Z-VAD-FMK and caspase 8 inhibitor Z-IETD-FMK were purchased from APEX BIO Technology Inc. (Houston, TX, USA). 2',7'-Dichlorodihydrofluorescein diacetate (DCFH-DA) were purchased from Merck Inc. (Darmstadt, Germany).

Table 1. The sequences of primers were used in this study.

Name	Sequences
hICAD-EcoRF	5'-CCGGAATTCATGGAGGTGACCGGGGACGCCGGGG-3'
hICAD-XhoR	5'-CCGCTCGAGCTATGTGGGATCCTGTCTGGCTCGC-3'
ICAD-M1-F	5'-CACCCAGGATCCCCGGAATTCATGGAGGTGACCGGGGACG-3'
ICAD-M1-R	5'-TGCCCCGCTTTCGTTCATCTACATCAAAGGACTC-3'
ICAD-M2-F	5'-ATGAAACAGAAAGCGGGGCAGGGTTGAAG-3'
ICAD-M2-R	5'-TACCCGTTTCTACTGCATCCACCTCCTCACCA-3'
ICAD-M3-F	5'-GGATGCAGTAGAAACGGGTATCAGCAGAGAGACC-3'
ICAD-M3-R	5'-CCCTCTAGATGCTATGCTCGAGCTATGTGGGATCCTGTCTGGCT-3'
ORF3-F	5'-TTTGCCTGTTTAAAGCGTCT-3'
ORF3-R	5'-AGTAAAAGCAGACTAAACAAAGCCT-3'
GAPDH-F	5'-AGGTCGGAGTCAACGGATTT-3'
GAPDH-R	5'-TAGTTGAGGTCAATGAAGGG-3'

2.3. Western-Blot Analysis

Whole-cell extracts were prepared with $2 \times$ SDS sample buffer (0.1 M Tris HCl, pH 6.8, 20% glycerol, 4% SDS, 10% β -Mercaptoethanol, 2% Bromophenol blue) and boiled for 10 min at 98 °C. Rabbit anti- γ H2AX (S139) (9718), -H2AX (2595), -pATM (S1981) (13050), -pChk2 (T68) (2661), -Chk2 (2662), -pChk1 (S317), -PARP (9542), -caspase 7 (9492), -cleaved caspase 3 (D175) (9661), mouse anti-DNA-PK (3H6), and -caspase 8 (9746) were purchased from Cell Signaling Technology (Danvers, MA, USA). Mouse anti-ATM (1A1), -Chk1 (G-4), -CAD (F-11), goat anti-ATR (N-19), and rabbit anti-caspase 3 (H-277) were purchased from Santa Cruz Biotechnology (Dallas, TX, USA). Rabbit anti-pATR (T1989) was purchased from GeneTex (Irvine, CA, USA). Rabbit anti-pDNA-PK (S2056) was purchased from Abcam (Cambridge, UK). Mouse anti-Flag (M-2) was purchased from Sigma-Aldrich (St. Louis, MO, USA). Rabbit anti-actin (20536) was purchased from Proteintech Group (Rosemont, IL, USA). Rabbit anti-PEDV N was generated previously in our lab [26]. The horseradish peroxidase (HRP)-conjugated goat anti-rabbit IgG antibody and HRP-conjugated goat anti-mouse IgG antibody were purchased from MiliporeSigma (Merck Inc., Darmstadt, Germany).

2.4. RNA Isolation and Reverse Transcription (RT)-Polymerase Chain Reaction (PCR)

Total RNA was extracted using TRIzol reagent (MiliporeSigma, Merck Inc., Darmstadt, Germany), and the cDNA was obtained using the HiScript II Q RT SuperMix for qPCR (+gDNA wiper) following the manufacturer's instructions (Vazyme Biotech, Inc. Nanjing, China). The PCR was carried out with primers targeting *ORF3* and *GAPDH* listed in Table 1 using $2 \times$ Taq Master Mix (Vazyme Biotech, Inc., Nanjing, China) under the following conditions: denaturation at 94 °C for 5 min, followed by 25 cycles of 94 °C for 30 s, annealing at 55 °C for 30 s, extension at 72 °C for 30 s, and a final extension at 72 °C for 10 min.

2.5. Indirect Immunofluorescence Assay (IFA)

IFA was performed as previously described [26]. Briefly, Vero-E6 cells were seeded at 8×10^5 on glass coverslips in a six-well plate, followed by mock-treated or infected with PEDV (MOI = 1) for indicated times. Cells were fixed and stained with their respective antibodies and visualized by the confocal microscope (Nikon Inc., Tokyo, Japan).

2.6. Transient Transfection and siRNA Knockdown

The experiments were performed as previously described [27]. siRNAs against *caspase-3*, *caspase-7*, *ATM*, *Chk2*, *H2AX*, and scramble siRNA are listed in Table 2 (Biotend Inc., Shanghai, China).

Table 2. The sequences of siRNA were used in this study.

Name	Sequences
siCaspase 3-1	GGA CUG UGG UAU UGA GAC A
siCaspase 3-2	GAA GGU AGC AAC AGA AUU U
siCaspase 7-2	UCG AAA CGG AAC AGA CAA A
siATM-1	GCA GAA AUC UAU GCA GAU A
siATM-2	UGA UAG AGC UAC AGA ACG A
siChk2-1	GGA CUC AAG UGU CAC UGA A
siChk2-2	CCU CUC UCA UGA GAA CCU U
siH2AX-1	ACA AGA AGA CGC GAA UCAU
siH2AX-2	ACG ACG AGG AGC UCA ACA A

2.7. ROS Analysis

Vero-E6 or Marc145 cells were infected with PEDV at different times and harvested at the same time. Then, cells were incubated with 10 μ M 2',7'-Dichlorodihydrofluorescein diacetate (DCFH-DA) at 37 °C for 30 min in dark. After rinsing three times with PBS, cells were trypsinized and resuspended in PBS and then analyzed by FACS Calibur flow cytometer (BD Biosciences Inc., San Jose, CA, USA).

2.8. Plaque Formation Assay

Vero-E6 cells were seeded in six-well plates at 80% confluence 18 h before infection. The virus was diluted in DMEM through serial ten-fold dilution and incubated with cells at 37 °C for 1 h. Cells were washed with PBS and overlaid with 1% low-melting-point agarose (Lonza Inc., Basel, Switzerland) in the DMEM medium with 2% FBS and incubated at 37 °C for 2–3 days until the plaques formed and finally stained with 0.5% crystal violet.

2.9. Cell Viability Analysis

The cytotoxicity of DNA damage inhibitors was measured by CCK-8 assay following the manufacturer's instructions (APExBIO, Houston, TX, USA). Briefly, Vero-E6 cells were seeded in the 96-well plate at 5000 per well for 12 h and then treated with an increased dose of inhibitors for 24 h, followed by incubated with CCK-8 reagent (10 μ L/well) at 37 °C for 4 h. Finally, the absorbance at 450 nm was measured in an enzyme-linked immunosorbent assay reader.

2.10. Statistical Analysis

The data were obtained from three replicates and presented as means \pm standard deviations (SD). Statistical significance between different groups was determined using the Student's *t*-test in GraphPad Prism 7.0 software (San Diego, CA, USA) (* $p < 0.05$; ** $p < 0.01$; *** $p < 0.001$).

3. Results

3.1. PEDV Infection Activates the ATM-Chk2 Signaling Pathway

To determine whether PEDV infection regulates host DNA damage response (DDR), we first examined the activation of three apical kinases ATM, ATR, and DNA-PK, and their downstream effectors in Vero-E6 cells infected with CV777 or HLJBY. We found that both PEDV strains dramatically induced ATM phosphorylation on Ser1981, ATR phosphorylation on Thr1989, ATM substrate Chk2 phosphorylation on Thr68, and H2AX phosphorylation on Ser139 (γ H2AX) at the late infection stage (Figure 1A,B), consistent with the previous observation in Vero cells upon infection with an epidemic PEDV strain SHpd/2012 [28]. However, DNA-PK phosphorylation on Ser2056 was not consistently affected by CV777 or HLJBY infection (Figure 1A,B). In contrast, UV-inactivated PEDV did not affect DDR-related proteins (Figure 1A), indicating that active virus replication is essential in order to activate cellular DDA. Similarly, we observed increased levels of phospho-ATM, phospho-Chk2, and γ H2AX but not phospho-ATR in CV777-infected

Marc145 cells (Figure 1C), demonstrating that PEDV infection-induced ATM signaling was not cell-type-specific. In addition, the proteolytic cleavage of PARP increased concomitantly with γ H2AX at 36 hpi in both Vero-E6 and Marc145 cells (Figure 1A–C), implying that γ H2AX probably correlates with the activation of caspases and apoptosis at the late stage of infection.

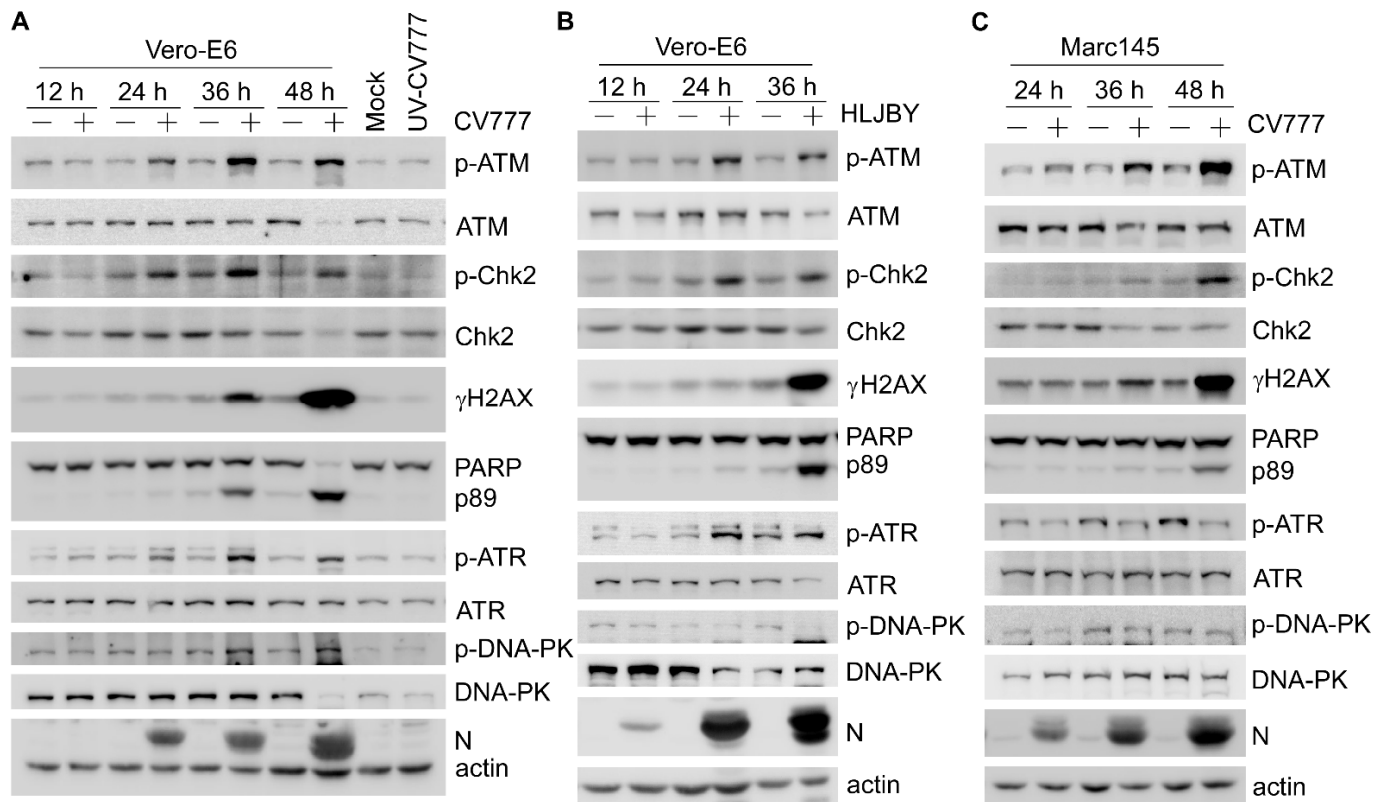


Figure 1. PEDV infection activates ATM-dependent DNA damage response. (A) Western blots were prepared with extracts from Vero-E6 cells uninfected or infected with CV777 (0.1 MOI) for 12, 24, 36, and 48 h. The levels of p-ATM (S1981), total ATM, p-Chk2(T68), total Chk2, p-ATR(T1989), total ATR, p-DNA-PK(S2056), total DNA-PK, γ H2AX, PEDV N, and actin were determined using their respective antibodies. Vero-E6 cells infected with UV-inactivated CV777 (0.1 MOI) for 48 h were used as the negative control. (B) Western blots were prepared with extracts from Vero-E6 cells uninfected or infected with HLJBY (0.1 MOI) for 12, 24, and 36 h. (C) Western blots were prepared with extracts from Marc145 cells uninfected or infected with CV777 (0.1 MOI) for 24, 36, and 48 h at 0.1 MOI.

3.2. Inhibition of ATM or Chk2 Suppresses PEDV Early Replication

Since both phospho-ATM and -ATR were activated in Vero-E6 cells upon PEDV infection, we examined the effect of KU55933 (ATM-specific inhibitor) and VE821 (ATR-specific inhibitor) on PEDV replication to determine the role of DDR kinases in regulating viral replication. First, the CCK-8 assay was performed in Vero-E6 cells treated with an increasing dose of KU55933 or VE821 and showed that cell viability was not affected by tested concentrations of both inhibitors (Figure S1A,B). Next, the levels of DDR and viral proteins were examined by Western blot. We found that PEDV-induced accumulation of phospho-ATM/ATR and -Chk2/Chk1 were dramatically attenuated by KU55933/VE821 treatment at 12 to 30 hpi (Figures 2A,B and S1C,D). However, the expression levels of PEDV N were decreased at 12 to 30 hpi by KU55933 (Figures 2A and S1C), but not VE821 treatment (Figures 2B and S1D). PEDV ORF3 gene is related to viral replication [29,30]. Thus, mRNA levels of ORF3 and extracellular virus titers were examined. We showed that the levels of ORF3 mRNA and PEDV titers were only decreased in KU55933-treated cells at 12 and 24 hpi (Figures S1E,F and 2C). Meanwhile, we also noticed that this inhibitory effect

of KU55933 gradually compromised along with increased infection time, indicating that the ATM kinase mainly contributes to PEDV replication at the early stage. To determine which factor of the ATM signaling pathway was involved in PEDV early replication, the protein level of PEDV N was measured in the presence or absence of ATM or Chk2. The results showed that knockdown of ATM/Chk2 led to reduced expression of PEDV N at 6 and 12 hpi (Figures 2D,E and S2A,B). Consistently, the PEDV titers at 6 and 12 hpi were also decreased when ATM was knocked down (Figure 2F). However, the reduction of PEDV titers was less pronounced at 12 hpi than 6 hpi upon knockdown of ATM, suggesting ATM was involved in the early stage of viral life cycle. In addition, the PEDV titers were slightly decreased by Chk2 knockdown at 6 hpi, but not at 12 hpi (Figure 2G), indicating Chk2 as a downstream effector of ATM plays a minor role in viral replication. Collectively, these findings indicated that ATM might play a role in the early stage of PEDV replication.

3.3. The Level of Phospho-ATM Is Correlated with PEDV-Induced ROS

Previous reports showed that PEDV infection induces reactive oxygen species (ROS) production and leads to apoptosis and autophagy [31,32]. ROS are the byproduct of mitochondrial physiological activities and able to stimulate DNA damage. To explore the role of ROS in PEDV-induced DDR, we examined the cellular ROS level in PEDV-infected cells. The results revealed the robust activation of ROS production in Vero-E6 (Figure 3A,B) and Marc145 cells (Figure 3C) upon PEDV infection. Next, PEDV-induced ROS production was analyzed by using three antioxidants, including apocynin (APO), an Nicotinamide adenine dinucleotide phosphate (NADPH) oxidase inhibitor, diphenyleneiodonium chloride (DPI), an inhibitor of NADPH oxidase and iNOS/eNOS, and N-acetylcysteine (NAC), a scavenger of free radicals especially oxygen radicals [33]. We showed that PEDV-induced accumulation of ROS was reduced by about 40% by APO treatment (46.3% in CV777 vs. 27.7% in APO+CV777), but was not affected by NAC treatment (Figure 3D,E). Surprisingly, the level of PEDV-induced ROS increased by around 62.2% in DPI-treated cells (46.3% in CV777 vs. 75.1% in DPI+CV777) (Figure 3D,E). Consistently, phospho-ATM exhibited the same trend as the cellular ROS level in control or PEDV-infected cells treatment with mock, APO, NAC, or DPI (Figure 3F). Surprisingly, we noticed that the levels of cleaved PARP and γ H2AX were decreased concurrently in DPI-treated cells at 30 hpi regardless of increased phospho-ATM (Figure 3F), implying the existence of other factors in regulating H2AX phosphorylation. Given that the level of cleaved PARP and γ H2AX changed simultaneously (Figures 1 and 3F), we speculated that γ H2AX was associated with the status of apoptosis. To address this, we examined the caspases' cleavage upon antioxidants treatment, including executioner caspase-3 and -7 as well as the initiator caspase-8. As expected, the levels of cleaved caspase-3, -7, and -8 were decreased concomitantly with the reduced accumulation of γ H2AX upon DPI treatment, but not APO or NAC treatment (Figure 3G).

3.4. PEDV Infection Induces a Confluent Pattern of γ H2AX-Nuclear Staining

Typical γ H2AX foci by IFA have been widely used as a biomarker of DNA double-strand breaks (DSBs) upon treatment with genotoxic reagents or irradiation [34]. Therefore, we analyzed the nuclear immunostaining of γ H2AX in PEDV-infected Vero-E6 cells (Figure 4A). Unlike etoposide, a topoisomerase II inhibitor, induced bright punctate γ H2AX foci distributed throughout the nucleus, PEDV-induced γ H2AX staining tended to be a confluent pattern that could be subdivided into three phases (Figure 4B, upper panel), including phase I (nuclear ring staining), phase II (pan-nuclear staining), and phase III (co-staining with shrunken apoptotic bodies), which highly resembled TNF-related apoptosis-inducing ligand (TRAIL)-induced γ H2AX activation [35,36]. Quantification of γ H2AX staining in each phase showed that over 40% were nuclear γ H2AX staining; among these, around 80% of γ H2AX positive cells were in phases II and III, consistent with the progression of cell death upon PEDV infection (Figure 4B, lower panel).

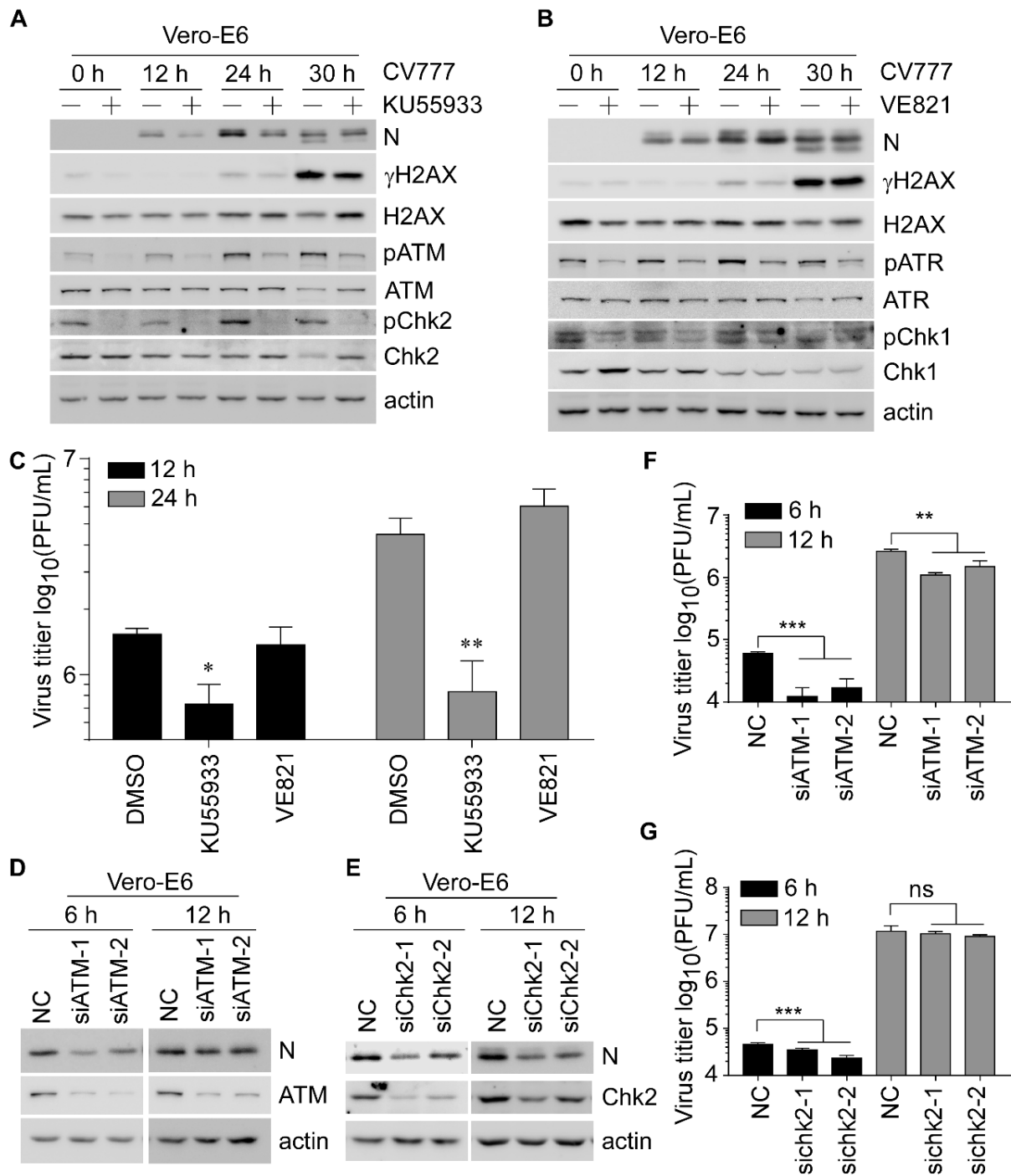


Figure 2. Suppression of the ATM signaling pathway inhibits the replication of PEDV. (A,B) Western blots were prepared with extracts from Vero-E6 cells pretreated with DMSO, ATM antagonist KU55933 (6 μ M) (A), or ATR antagonist VE821 (2 μ M) (B) for 2 h and followed by infection with CV777 (0.5 MOI) in the presence of DMSO or KU55933 (A), or VE821 (B) for 12, 24, 30 h. (C) The virus titers were measured by PFU assay with supernatants harvested from Vero-E6 cells pretreated with DMSO or KU55933 (6 μ M) or VE821 (2 μ M) for 2 h before and during infection with CV777 (0.1 MOI) for 12 and 24 h. (D,E) Western blots were prepared with extracts from Vero-E6 cells transfected with scramble or 50 nM siATM (D), or siChk2 (E) for 48 h and followed by infection with 0.1 MOI CV777 for 6 and 12 h. (F,G) The experiment was performed as in (D,E), except the cells and supernatants were collected for PFU assay (* $p < 0.05$; ** $p < 0.01$; *** $p < 0.001$).

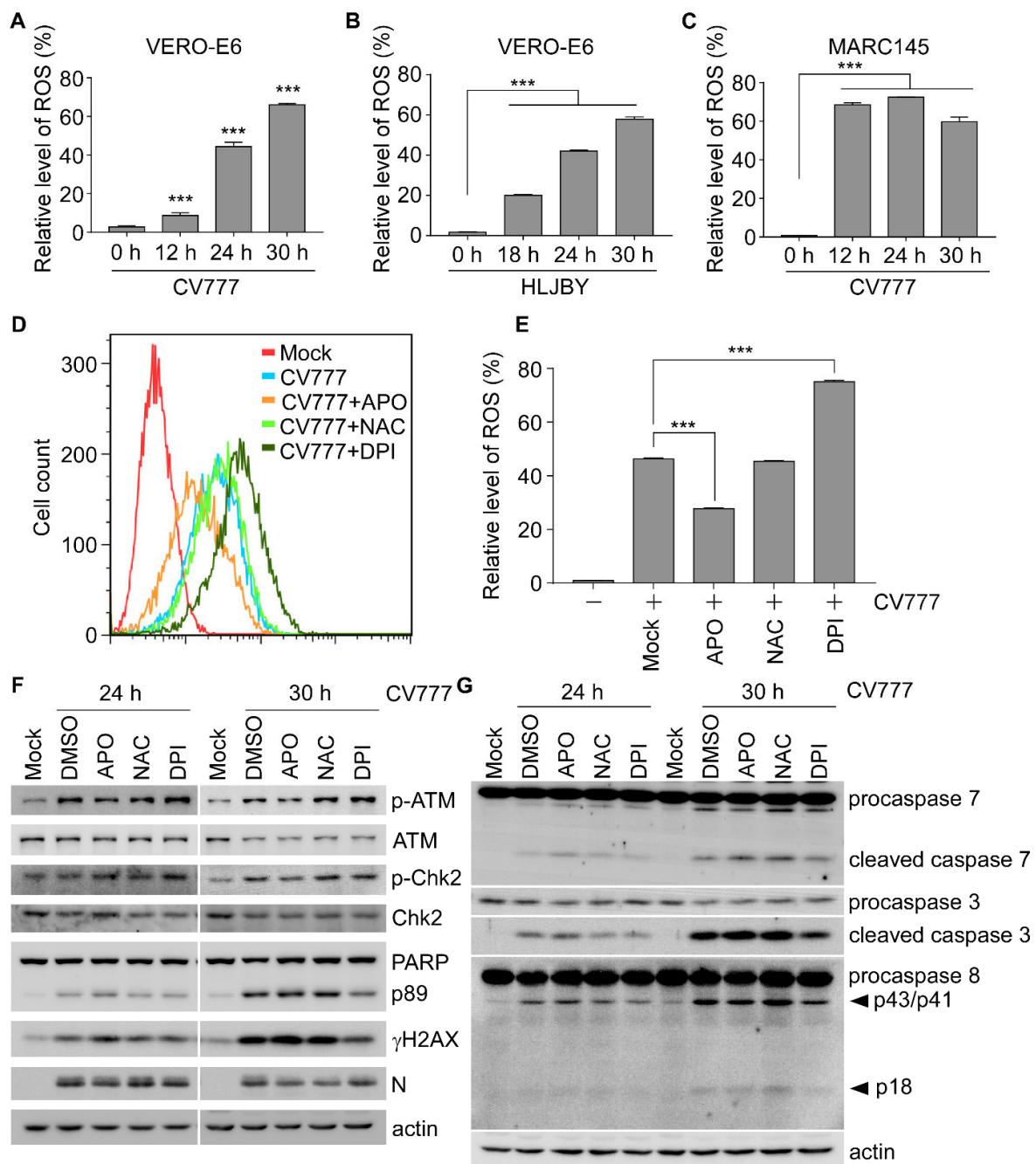


Figure 3. PEDV-induced cellular ROS contributes to the activation of the ATM signaling. **(A)** ROS levels were measured with Vero-E6 cells uninfected or infected with CV777 (1 MOI) for 12, 24, and 30 h. The relative ROS levels were calculated by the DCF fluorescence intensity in PEDV-infected cells. Results are representative of three independent experiments. **(B)** ROS levels were measured with Vero-E6 cells uninfected or infected with HLJBY (1 MOI) at 18, 24, and 30 h. **(C)** The experiment was performed as in A, except using Marc145 cells. **(D)** ROS levels were measured in Vero-E6 cells pre-treated with DMSO, APO (1 mM), NAC (100 μ M), or DPI (0.5 μ M) for 2 h and followed by CV777 (1 MOI) infection in the presence of DMSO, APO (1 mM), NAC (100 μ M), or DPI (0.5 μ M) for 24 h. **(E)** The quantification of the relative ROS levels calculated by the DCF fluorescence intensity in cells that were treated as in **(D)**. Results are representative of three independent experiments. **(F,G)** Western blots were prepared with extracts from Vero-E6 cells treated with DMSO, APO (1 mM), NAC (100 μ M), or DPI (0.5 μ M) for 2 h before and during infection with CV777 (1 MOI) for 24 and 30 h (***) $p < 0.001$.

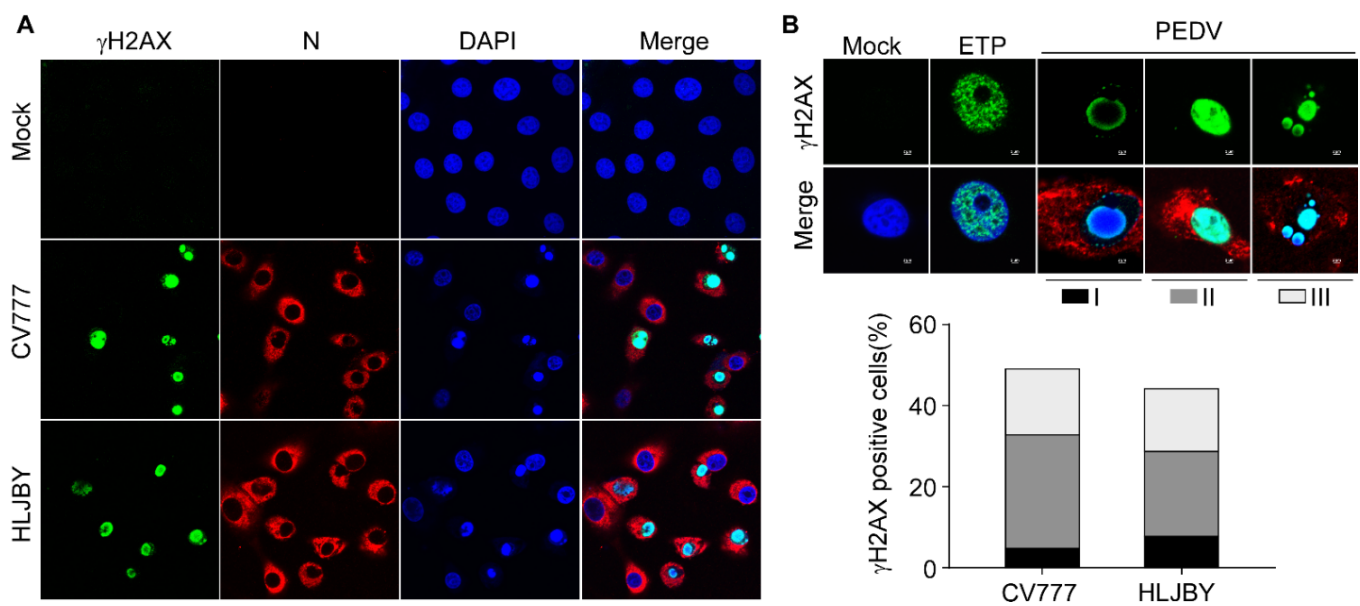


Figure 4. The pan-nuclear staining of γ H2AX in PEDV-infected Vero-E6 cells. (A) Confocal images are representative of γ H2AX immunofluorescence staining in Vero-E6 cells infected with PEDV (1 MOI) for 30 h. γ H2AX was labeled in green, PEDV N was labeled in red, and nuclei were stained in blue with DAPI. (B) Representative confocal images of a single cell showing the γ H2AX patterns in different phases (600 \times magnification). From left to right: untreated cells, etoposide-treated cells, and CV777 infected cells. The graph shows the relative distribution of the different γ H2AX patterns (over 100 cells). Black columns correspond to peripheral nuclear staining (ring pattern, I), dark gray columns correspond to pan-staining (flooded pattern, II), and light gray columns correspond to apoptotic bodies fully stained with γ H2AX (III).

3.5. PEDV-Induced γ H2AX Is Associated with Caspase Activation

To determine the role of caspases in PEDV-induced H2AX phosphorylation, Vero-E6 cells were treated with the pan-caspase inhibitor Z-VAD-FMK, and we found that γ H2AX was dramatically decreased along with reduced cleavage of caspase-3, -7, and -8, in Z-VAD-FMK-treated cells in a dose-dependent manner, while phospho-ATM and -Chk2 were not affected (Figure 5A). Next, to determine which caspase is involved in regulating H2AX phosphorylation, Vero-E6 cells were treated with Z-IETD-FMK (a caspase-8 inhibitor) and Ac-DEVD-CHO (a caspase-3/7 inhibitor). We found that both inhibitors exerted similar inhibitory effects on γ H2AX, but not phospho-ATM and -Chk2, suggesting that PEDV-induced γ H2AX was associated with caspase activity but not phospho-ATM and -Chk2 (Figure 5B). However, the levels of cleaved caspase-3, -7, and -8 were decreased in Z-IETD-FMK-treated cells, while only caspase-3 and -7 were inhibited in Ac-DEVD-CHO-treated cells, indicating that caspase-3/-7 might contribute to the PEDV-induced H2AX phosphorylation (Figure 5B). Next, we also analyzed the γ H2AX staining and found the percentage of γ H2AX positive cells was significantly decreased by caspase inhibitors (Figures 5C and S3). To further clarify the major caspase involved in this regulation, caspase-3 or -7 was transiently knocked down by siRNA in Vero-E6 cells. We showed that PEDV-induced γ H2AX was only inhibited in caspase-7 knockdown cells (Figure 5D,E), suggesting that caspase-7 is a key factor that mediates PEDV-induced H2AX phosphorylation. Taken together, these data demonstrate that PEDV regulates H2AX phosphorylation through activating caspase-7 rather than the classical ATM-Chk2 signaling pathway.

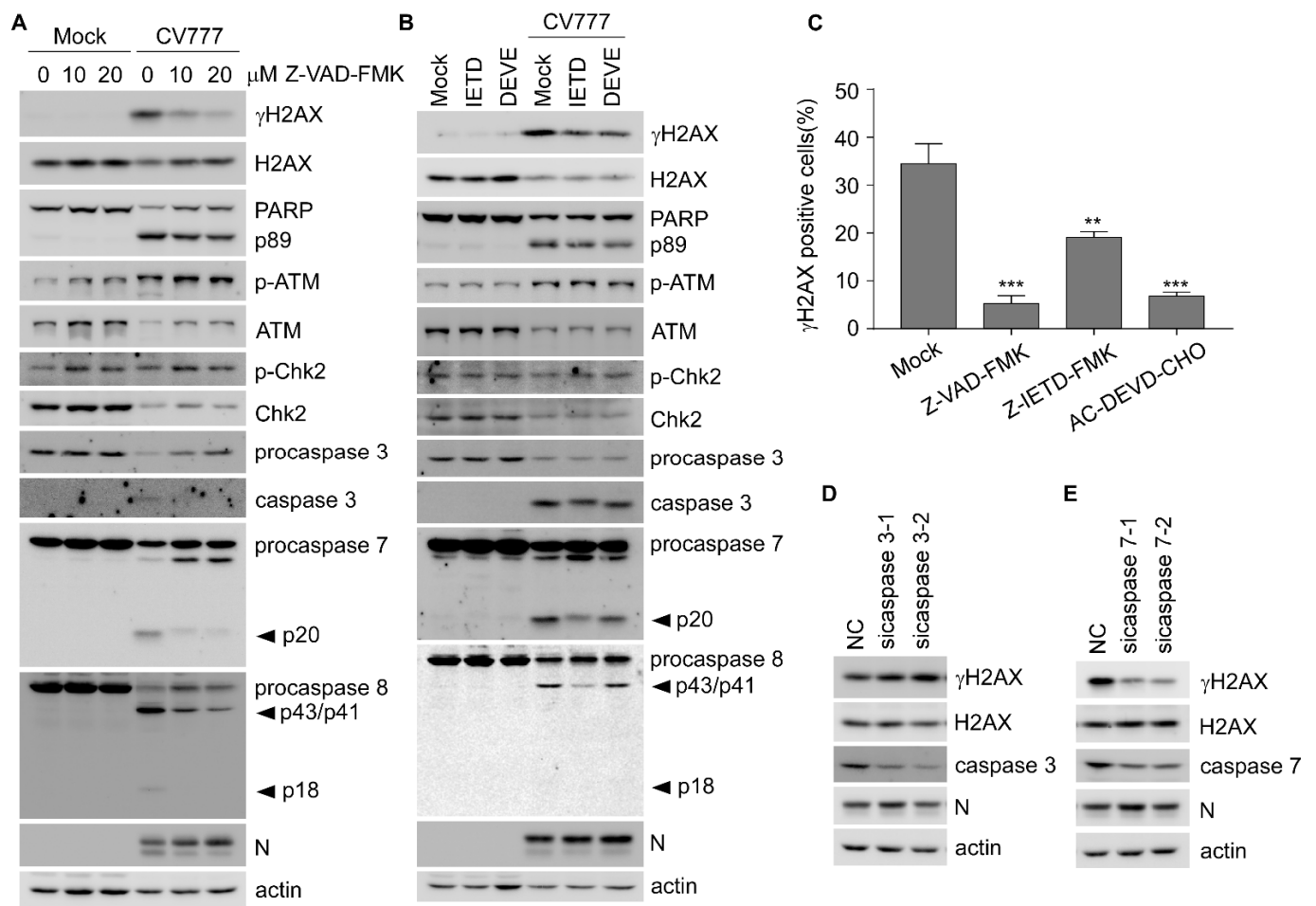


Figure 5. PEDV-induced phosphorylation of H2AX is decreased by caspase inhibitors. (A) Western blots were prepared with extracts from Vero-E6 cells treated with DMSO or caspase pan-inhibitor Z-VAD-FMK (0, 10, and 20 μ M) for 2 h before and during infection with CV777 (0.5 MOI) for 30 h. (B) Western blots were prepared with extracts from Vero-E6 cells treated with DMSO or caspase-8 inhibitor Z-IETD-FMK (50 μ M), or caspase-3/7 inhibitor Ac-DEVD-CHO (50 μ M) for 2 h before and during infection with CV777 (0.5 MOI) for 30 h. (C) IFA was performed with Vero-E6 cells treated with DMSO, Z-VAD-FMK (10 μ M), Z-IETD-FMK (50 μ M), and Ac-DEVD-CHO (50 μ M) for 2 h, respectively, before and during infection with CV777 (0.5 MOI) for 30 h. The cells were fixed and double-immunostained with specific rabbit anti- γ H2AX and mouse anti-N antibodies. The nuclei were stained with DAPI. The graph shows the percentage of γ H2AX positive cells in about 200 PEDV-infected cells. (D,E) Western blots were prepared with extracts from Vero-E6 cells transiently transfected with 50 nM scramble or caspase-3/7 siRNA for 48 h, followed by 1 MOI CV777 infection for 25 h (** $p < 0.01$; *** $p < 0.001$).

3.6. Caspase-Activated DNase Plays a Role in PEDV-Induced H2AX Phosphorylation

Caspases-3 and -7 can cleave the inhibitor of caspase-activated DNase (ICAD) and lead to dissociation of the caspase-activated DNase (CAD) from the CAD-ICAD complex to form the CAD homodimer, which acts as a DNA scissor to generate DSBs and initiate apoptosis [37]. Studies showed that PEDV induces apoptosis at the late stage of infection [24,38] and increases γ H2AX as a result of apoptotic DNA fragmentation [39]. To determine whether the activity of CAD is responsible for PEDV-induced γ H2AX, Vero-E6 cells were transfected with Flag-tagged ICAD or ICAD-M (D117E, D224E) and followed by the infection of CV777 or HLJBY. We showed that PEDV-induced γ H2AX was decreased in cells expressing ICAD and further decreased in cells expressing ICAD-M (Figure 6A,B), owing to the resistance of ICAD-M to caspase cleavage and form a stable inactive ICAD/CAD

in cells. Moreover, γ H2AX staining cells were also analyzed and showed that γ H2AX was abolished in cells expressing ICAD or ICAD-M (Figure 6C). To further confirm this, endogenous CAD was transiently knocked down in Vero-E6 cells. The results showed that knockdown of CAD attenuated CV777- or HLJBY-induced H2AX phosphorylation (Figure 6D,E). Therefore, these data demonstrated that CAD activity is involved in PEDV-induced H2AX phosphorylation.

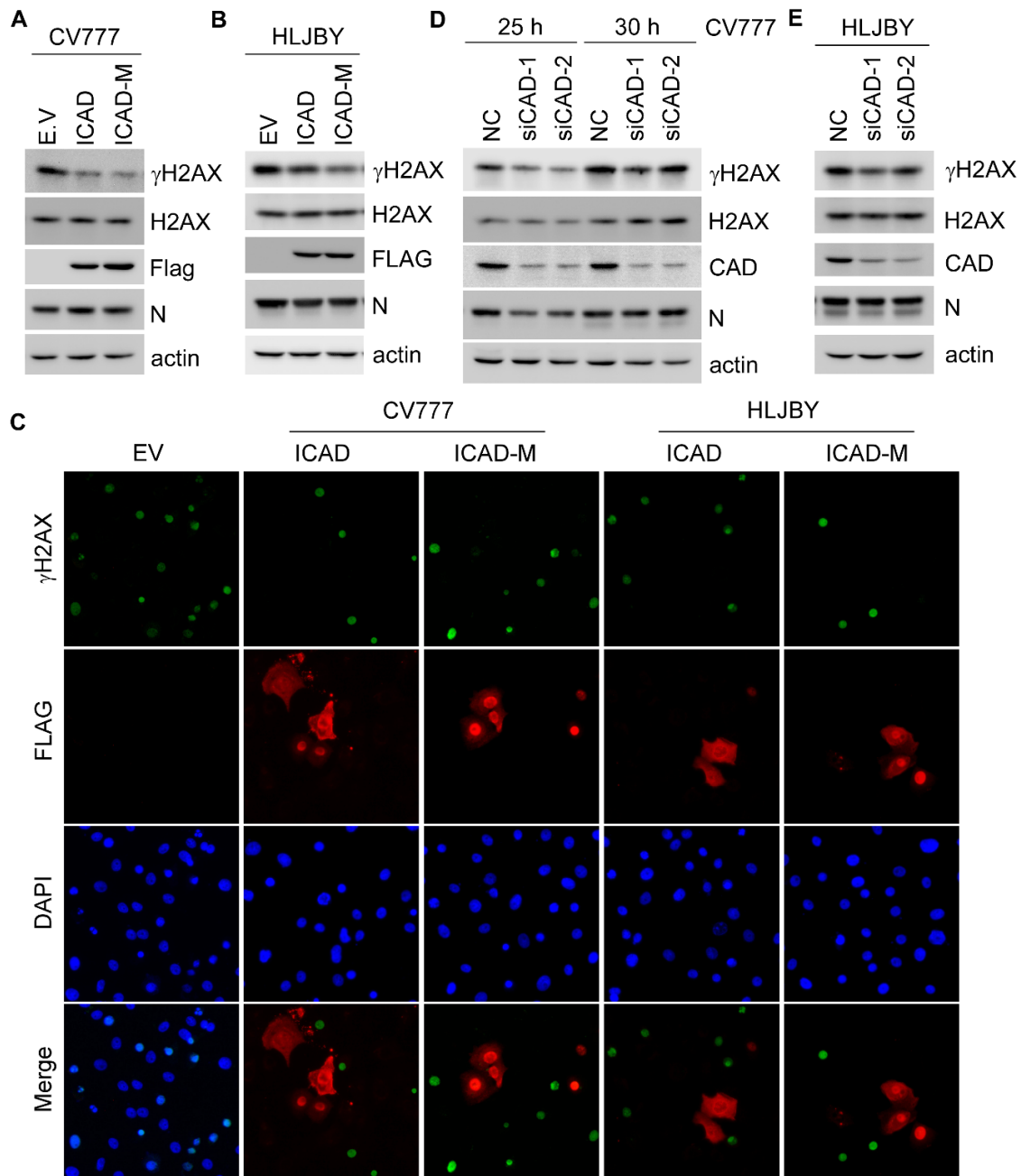


Figure 6. CAD implicates in PEDV-induced H2AX phosphorylation. (A,B) Western blots were prepared with extracts from Vero-E6 cells transiently transfected with empty vector or Flag-tagged ICAD or ICAD-M (D117E, D224E) for 30 h, followed by 1 MOI CV777 (A) or HLJBY (B) infection for 25 h. (C) IFA was performed with Vero-E6 cells transiently transfected with empty vector or Flag-tagged ICAD or ICAD-M (D117E, D224E) for 30 h, followed by 1 MOI CV777 infection for 25 h. (D,E) Western blots were prepared with extracts from Vero-E6 cells transiently transfected with 50 nM scramble or CAD siRNA for 48 h, followed by 1 MOI CV777 (D) or HLJBY (E) infection for 25 and 30 h.

3.7. H2AX Contributes to the PEDV Early Replication

The aforementioned studies showed that the PEDV-induced γ H2AX occurred simultaneously with caspase-7 activation in an ATM-independent manner. Therefore, we investigated the role of H2AX in PEDV replication. We observed a reduced expression of PEDV N at 6 and 12 hpi in H2AX-knockdown cells (Figure 7A,B). Virus propagation measured by PFU also showed decreased PEDV titers upon H2AX knockdown (Figure 7C). These data together indicated that H2AX plays a role in regulating PEDV early propagation.

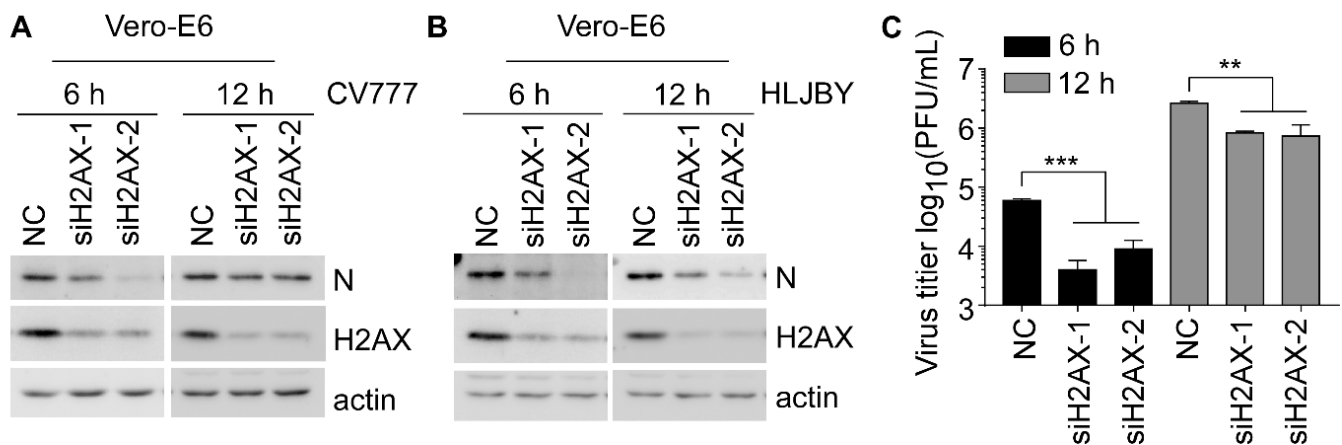


Figure 7. Silencing H2AX decreases PEDV replication. (A,B) Western blots were prepared with extracts from Vero-E6 cells transiently transfected with 50 nM scramble or H2AX siRNA for 48 h, followed by 1 MOI CV777 (A) or HLJBY (B) infection for 6 and 12 h. (C) Western blots were prepared with extracts from Vero-E6 cells transfected with 50 nM scramble or H2AX siRNA for 48 h, followed by 1 MOI CV777 infection for 6 and 12 h. The cells and supernatants were collected for PFU assay (** $p < 0.01$; *** $p < 0.001$).

4. Discussion

In this study, we described two distinct routes for PEDV to activate cellular DDR signaling molecules, phosphor-ATM and γ H2AX, to promote viral replication (Figure 8). We observed robust activation of phosphor-ATM, phosphor-ATR, and phosphor-Chk2 at 24 to 48 hpi in Vero-E6 cells, while inhibition of ATM, but not ATR kinase activity dramatically reduces viral replication. Consistently, knockdown of ATM or Chk2 moderately decreases PEDV replication at the early stage, indicating that activation of the ATM signaling is favorable for PEDV replication. In contrast to DNA viruses, such as herpes simplex virus (HSV), which triggers rapid DDR shortly after infection [40,41], RNA viruses such as Newcastle disease virus (NDV) and Zika virus elicit DDR at the relative late infection stage [42,43]. NDV induces ATM-Chk2 axis by membrane fusion mediated syncytium formation [42], while Zika virus induces DDR by replicating in the endoplasmic reticulum (ER) where excessive cytoplasmic ROS is produced [44]. In addition, HCV has also been shown to induce DDR through ROS and NOS accumulation [6,7]. Here, we found that PEDV infection activates the ATM signaling at the late infection stage. Like Zika virus and HCV, PEDV exclusively replicates in cytoplasmic convoluted membranes. Consistently, we found that PEDV-induced ATM activation is closely related to the level of cellular ROS, providing a possible explanation as to how single positive-strand RNA viruses (replicate in the cytoplasm) induce ATM-mediated DNA damage response.

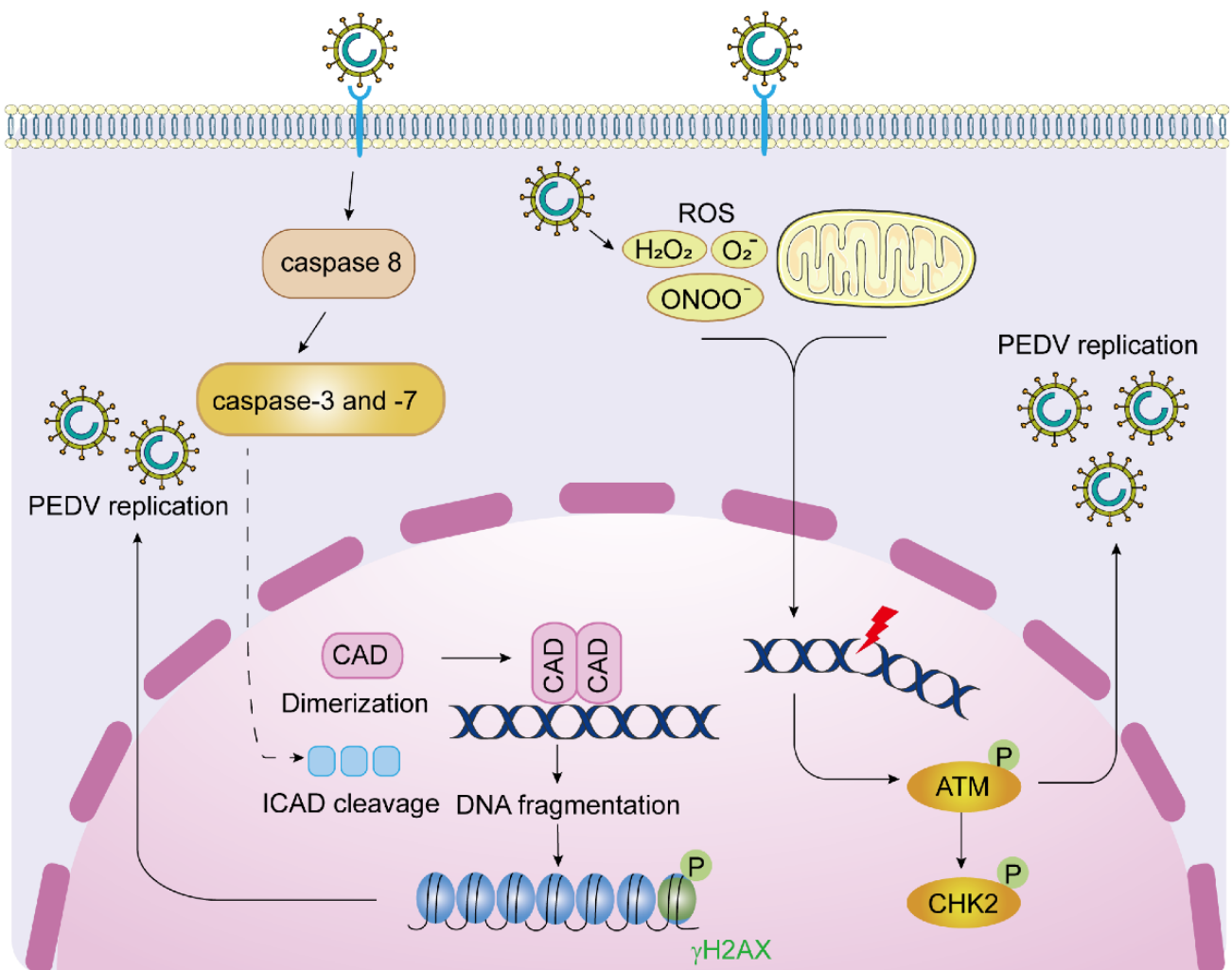


Figure 8. The interplay between PEDV replication and cellular DNA damage response. After PEDV enters host cells and replicates in the cytoplasm, the accumulation of massive intracellular ROS activates ATM-mediated DSB. Activated ATM and its downstream substrate Chk2 facilitate viral replication in the early infection stage. In the late stage of PEDV infection, the initiator caspase-8 activates the executioner caspase-3 and caspase-7 which subsequently cleave ICAD and release CAD from the ICAD-CAD complex and promote the homodimerization of CAD. The scissor-like CAD dimers create DSBs in the genome and DNA fragmentation, leading to H2AX phosphorylation in the nucleus. Inhibition of H2AX, ATM, and Chk2 dampens the replication of PEDV.

APO and DPI are NADPH oxidase inhibitors. NAC is a synthetic precursor of cysteine and glutathione and functions as a ROS scavenger. These inhibitors are applied in numerous studies to suppress oxidative stress, but the mechanisms of their activities are unclear. Surprisingly, our data suggested that only APO sufficiently decreased ROS, while NAC had little effect and DPI showed the opposite effect (Figure 3D,E). Consistently, there was evidence that DPI could exert the prooxidative functions in certain cell types and conditions [45–47]. DPI alters the redox metabolism by inhibiting the pentose phosphate pathway responsible for NADPH synthesis, thus making cells more prone to oxidative stress [46]. Therefore, the effects of inhibitors are largely cell-type and stimuli dependent; however, many studies neglected the importance of examining the actual ROS level upon inhibitors' treatment. In addition, DPI has also been shown to have a paradoxical effect on inducing apoptosis. For example, DPI promotes mitochondrial superoxide-mediated apoptosis [48], while inhibiting the sodium deoxycholate-mediated apoptosis [49]. DPI suppresses *H. pylori*-induced apoptosis and DNA fragmentation in gastric epithelial cells [50].

Consistently, our findings also suggest that DPI dramatically inhibits PEDV-induced cleavage of caspase-3, -7, -8, and PARP (Figure 3G), indicating the cytoprotective effect of DPI in response to PEDV infection.

Phosphorylation of H2AX, a variant of histone H2A, on serine 139 (γ H2AX) has been widely considered a DSB marker and is essential for DNA repair [51,52]. Aside from canonical functions, many researchers reported multiple non-canonical functions of H2AX, including senescence maintenance [53], chromatin regulation during mitosis [54], stem cell development [55,56], and apoptosis [39]. We found that PEDV induces robust H2AX phosphorylation concomitantly with PARP cleavage at 36 hpi, indicating the initiation of apoptosis (Figure 1). Interestingly, a unique γ H2AX nuclear staining pattern was observed which started with the perinuclear ring and evolved into pan-nuclear staining before and after nuclei undergo pyknosis, which highly resembles the γ H2AX staining in TRAIL-treated cells [34,35]. γ H2AX pan-nuclear staining is observed under many circumstances, including UV radiation [57,58], replicative stress and checkpoint abrogation [59,60], hypotonic treatment [61], ion irradiation [62], and viral infection [8,63,64]. Interestingly, TRAIL-induced activation of ATM and Chk2 can be blocked by a pan-caspase inhibitor [35], whereas treatment of Z-VAD-FMK efficiently decreases γ H2AX without affecting PEDV-induced phosphor-ATM and -Chk2, suggesting PEDV regulates H2AX phosphorylation independent of ATM activity. As the major executioner caspase, caspase-3 is considered to play a crucial role in regulating H2AX phosphorylation [65]. In addition, caspase-8 has also been shown to orchestrate H2AX phosphorylation [66]. Here, we demonstrate that activated caspase-7 is the key caspase in regulating H2AX phosphorylation upon PEDV infection. Next, we explored the connection between CAD activation and H2AX phosphorylation and for this regulation PEDV-induced H2AX phosphorylation was tightly related to CAD activation independent of ATM activity. Collectively, these findings extended our knowledge of the interaction between PEDV and host DNA damage response and shed light on the mechanisms of RNA viruses, especially coronaviruses, in regulating host DDR.

Supplementary Materials: The following supporting information can be downloaded at: <https://www.mdpi.com/article/10.3390/v14081782/s1>, Figure S1: The treatment of KU559333, not VE821 decreases PEDV replication; Figure S2: Knockdown of ATM or Chk2 inhibits PEDV replication; Figure S3: The percentage of PEDV-induced γ H2AX positive cells was decreased upon treatment with caspase inhibitors.

Author Contributions: Conceptualization, Y.-S.J. and Y.Q.; methodology, X.M. and H.C.; validation, X.M., H.C., Y.Y., P.Z. and C.Z.; formal analysis, X.M.; investigation, X.M., H.C., Y.Y., P.Z., C.Z. and L.S.; resources, L.S.; writing—original draft preparation, X.M.; writing—review and editing, H.-J.S., J.-S.L., Y.-S.J. and Y.Q.; visualization, X.M.; supervision, Y.-S.J. and Y.Q.; funding acquisition, H.C. and Y.Q. All authors have read and agreed to the published version of the manuscript.

Funding: This work was supported by the National Natural Science Foundation (31900141 and 31472218), the Fundamental Research Funds for the Central Universities (KJQN202022), and the Priority Academic Program Development of Jiangsu Higher Education Institutions (PAPD).

Institutional Review Board Statement: Not applicable.

Informed Consent Statement: Not applicable.

Data Availability Statement: Not applicable.

Acknowledgments: The authors would like to thank our laboratory members who helped us to improve the manuscript with their skillful technical assistance, invaluable comments, and suggestions.

Conflicts of Interest: The authors declare no conflict of interest.

Abbreviations

APO, Apocynin; ATM, Ataxia telangiectasia mutated; ATR, ATM and Rad3 related; CAD, Caspase-activated DNase; Chk1, Checkpoint kinase 1; Chk2, Checkpoint kinase 2; DDR, DNA damage response; DNA-PK, DNA-dependent protein kinase; DPI, Diphenyleneiodonium chloride; DSB,

DNA double-strand break; H2AX, Histone H2AX; HCV, Hepatitis C virus; HU, Hydroxyurea; IBV, Infectious bronchitis virus; NAC, N-Acetylcysteine; NADPH, Nicotinamide adenine dinucleotide phosphate; NO, Nitric oxide; NOS, Nitric oxide synthase; PARP, Poly (ADP-ribose) polymerase; PEDV, Porcine epidemic diarrhea virus; PFU, Plaque-forming unit; ROS, Reactive oxygen species; TRAIL, TNF-related apoptosis-inducing ligand.

References

- Zhou, B.B.; Elledge, S.J. The DNA damage response: Putting checkpoints in perspective. *Nature* **2000**, *408*, 433–439. [[CrossRef](#)] [[PubMed](#)]
- Roos, W.P.; Kaina, B. DNA damage-induced cell death by apoptosis. *Trends Mol. Med.* **2006**, *12*, 440–450. [[CrossRef](#)] [[PubMed](#)]
- Sulli, G.; Di Micco, R.; di Fagagna, F.D.A. Crosstalk between chromatin state and DNA damage response in cellular senescence and cancer. *Nat. Rev. Cancer* **2012**, *12*, 709–720. [[CrossRef](#)] [[PubMed](#)]
- Harper, J.W.; Elledge, S.J. The DNA damage response: Ten years after. *Mol. Cell* **2007**, *28*, 739–745. [[CrossRef](#)] [[PubMed](#)]
- Ryan, E.L.; Hollingworth, R.; Grand, R.J. Activation of the DNA Damage Response by RNA Viruses. *Biomolecules* **2016**, *6*, 2. [[CrossRef](#)] [[PubMed](#)]
- Machida, K.; Cheng, K.T.-H.; Sung, V.M.-H.; Lee, K.J.; Levine, A.M.; Lai, M.M.C. Hepatitis C Virus Infection Activates the Immunologic (Type II) Isoform of Nitric Oxide Synthase and Thereby Enhances DNA Damage and Mutations of Cellular Genes. *J. Virol.* **2004**, *78*, 8835–8843. [[CrossRef](#)]
- Machida, K.; Cheng, K.T.-H.; Lai, C.-K.; Jeng, K.-S.; Sung, V.M.-H.; Lai, M.M.C. Hepatitis C Virus Triggers Mitochondrial Permeability Transition with Production of Reactive Oxygen Species, Leading to DNA Damage and STAT3 Activation. *J. Virol.* **2006**, *80*, 7199–7207. [[CrossRef](#)]
- Xu, L.H.; Huang, M.; Fang, S.G.; Liu, D.X. Coronavirus Infection Induces DNA Replication Stress Partly through Interaction of Its Nonstructural Protein 13 with the p125 Subunit of DNA Polymerase δ . *J. Biol. Chem.* **2011**, *286*, 39546–39559. [[CrossRef](#)]
- Victor, J.; Deutsch, J.; Whitaker, A.; Lamkin, E.N.; March, A.; Zhou, P.; Botten, J.W.; Chatterjee, N. SARS-CoV-2 triggers DNA damage response in Vero E6 cells. *Biochem. Biophys. Res. Commun.* **2021**, *579*, 141–145. [[CrossRef](#)]
- Pensaert, M.B.; de Bouck, P. A new coronavirus-like particle associated with diarrhea in swine. *Arch. Virol.* **1978**, *58*, 243–247. [[CrossRef](#)]
- Song, D.; Park, B. Porcine epidemic diarrhoea virus: A comprehensive review of molecular epidemiology, diagnosis, and vaccines. *Virus Genes* **2012**, *44*, 167–175. [[CrossRef](#)]
- Kocherhans, R.; Bridgen, A.; Ackermann, M.; Tobler, K. Completion of the Porcine Epidemic Diarrhoea Coronavirus (PEDV) Genome Sequence. *Virus Genes* **2001**, *23*, 137–144. [[CrossRef](#)]
- Stevenson, G.W.; Hoang, H.; Schwartz, K.J.; Burrough, E.R.; Sun, D.; Madson, D.; Cooper, V.L.; Pillatzki, A.; Gauger, P.; Schmitt, B.J.; et al. Emergence of Porcine epidemic diarrhoea virus in the United States: Clinical signs, lesions, and viral genomic sequences. *J. Vet. Diagn. Investig.* **2013**, *25*, 649–654. [[CrossRef](#)]
- Lin, C.-N.; Chung, W.-B.; Chang, S.-W.; Wen, C.-C.; Liu, H.; Chien, C.-H.; Chiou, M.-T. US-Like Strain of Porcine Epidemic Diarrhoea Virus Outbreaks in Taiwan, 2013–2014. *J. Vet. Med. Sci.* **2014**, *76*, 1297–1299. [[CrossRef](#)]
- Lee, S.; Lee, C. Outbreak-Related Porcine Epidemic Diarrhoea Virus Strains Similar to US Strains, South Korea, 2013. *Emerg. Infect. Dis. J.* **2014**, *20*, 1223. [[CrossRef](#)]
- Ojkic, D.; Hazlett, M.; Fairles, J.; Marom, A.; Slavic, D.; Maxie, G.; Alexandersen, S.; Pasick, J.; Alsop, J.; Burlatschenko, S. The first case of porcine epidemic diarrhoea in Canada. *Can. Vet. J.* **2015**, *56*, 149–152.
- Xu, X.; Wang, L.; Liu, Y.; Shi, X.; Yan, Y.; Zhang, S.; Zhang, Q. TRIM56 overexpression restricts porcine epidemic diarrhoea virus replication in Marc-145 cells by enhancing TLR3-TRAF3-mediated IFN- β antiviral response. *J. Gen. Virol.* **2022**, *103*, 001748. [[CrossRef](#)]
- Yan, Q.; Liu, X.; Sun, Y.; Zeng, W.; Li, Y.; Zhao, F.; Wu, K.; Fan, S.; Zhao, M.; Chen, J.; et al. Swine Enteric Coronavirus: Diverse Pathogen-Host Interactions. *Int. J. Mol. Sci.* **2022**, *23*, 3953. [[CrossRef](#)]
- Zhang, K.; Lin, S.; Li, J.; Deng, S.; Zhang, J.; Wang, S. Modulation of Innate Antiviral Immune Response by Porcine Enteric Coronavirus. *Front. Microbiol.* **2022**, *13*, 845137. [[CrossRef](#)]
- Li, S.; Yang, F.; Ma, C.; Cao, W.; Yang, J.; Zhao, Z.; Tian, H.; Zhu, Z.; Zheng, H. Porcine epidemic diarrhoea virus nsp14 inhibits NF- κ B pathway activation by targeting the IKK complex and p65. *Anim. Dis.* **2021**, *1*, 24. [[CrossRef](#)]
- Li, S.; Zhu, Z.; Yang, F.; Cao, W.; Yang, J.; Ma, C.; Zhao, Z.; Tian, H.; Liu, X.; Ma, J.; et al. Porcine Epidemic Diarrhoea Virus Membrane Protein Interacted with IRF7 to Inhibit Type I IFN Production during Viral Infection. *J. Immunol.* **2021**, *206*, 2909–2923. [[CrossRef](#)] [[PubMed](#)]
- Lu, Y.; Cai, H.; Lu, M.; Ma, Y.; Li, A.; Gao, Y.; Zhou, J.; Gu, H.; Li, J.; Gu, J. Porcine Epidemic Diarrhoea Virus Deficient in RNA Cap Guanine-N-7 Methylation Is Attenuated and Induces Higher Type I and III Interferon Responses. *J. Virol.* **2020**, *94*, e00447-20. [[CrossRef](#)] [[PubMed](#)]
- Kim, Y.; Lee, C. Porcine epidemic diarrhoea virus induces caspase-independent apoptosis through activation of mitochondrial apoptosis-inducing factor. *Virology* **2014**, *460–461*, 180–193. [[CrossRef](#)] [[PubMed](#)]

24. Zhang, X.; Li, P.; Zheng, Q.; Hou, J. Lactobacillus acidophilus S-layer protein-mediated inhibition of PEDV-induced apoptosis of Vero cells. *Vet. Microbiol.* **2019**, *229*, 159–167. [[CrossRef](#)]
25. Oh, C.; Kim, Y.; Chang, K.-O. Caspase-mediated cleavage of nucleocapsid protein of a protease-independent porcine epidemic diarrhea virus strain. *Virus Res.* **2020**, *285*, 198026. [[CrossRef](#)]
26. Sun, L.; Chen, H.; Ming, X.; Bo, Z.; Shin, H.-J.; Jung, Y.-S.; Qian, Y.; Gallagher, T. Porcine Epidemic Diarrhea Virus Infection Induces Caspase-8-Mediated G3BP1 Cleavage and Subverts Stress Granules To Promote Viral Replication. *J. Virol.* **2021**, *95*, e02344-20. [[CrossRef](#)]
27. Ming, X.; Bo, Z.; Miao, Y.; Chen, H.; Bao, C.; Sun, L.; Xi, R.; Zhong, Q.; Zhao, P.; Jung, Y.-S.; et al. Pseudorabies virus kinase UL13 phosphorylates H2AX to foster viral replication. *FASEB J.* **2022**, *36*, e22221. [[CrossRef](#)]
28. Luo, Y.R.; Zhou, S.T.; Yang, L.; Liu, Y.P.; Jiang, S.Y.; Dawuli, Y.; Hou, Y.X.; Zhou, T.X.; Yang, Z.B. Porcine Epidemic Diarrhoea Virus Induces Cell-cycle Arrest through the DNA Damage-signalling Pathway. *J. Vet. Res.* **2020**, *64*, 25–32. [[CrossRef](#)]
29. Wang, K.; Lu, W.; Chen, J.; Xie, S.; Shi, H.; Hsu, H.; Yu, W.; Xu, K.; Bian, C.; Fischer, W.B.; et al. PEDV ORF3 encodes an ion channel protein and regulates virus production. *FEBS Lett.* **2012**, *586*, 384–391. [[CrossRef](#)]
30. Kaewborisuth, C.; He, Q.; Jongkaewwattana, A. The Accessory Protein ORF3 Contributes to Porcine Epidemic Diarrhea Virus Replication by Direct Binding to the Spike Protein. *Viruses* **2018**, *10*, 399. [[CrossRef](#)]
31. Xu, X.; Xu, Y.; Zhang, Q.; Yang, F.; Yin, Z.; Wang, L.; Li, Q. Porcine epidemic diarrhea virus infections induce apoptosis in Vero cells via a reactive oxygen species (ROS)/p53, but not p38 MAPK and SAPK/JNK signalling pathways. *Vet. Microbiol.* **2019**, *232*, 1–12. [[CrossRef](#)]
32. Sun, P.; Jin, J.; Wang, L.; Wang, J.; Zhou, H.; Zhang, Q.; Xu, X. Porcine epidemic diarrhea virus infections induce autophagy in Vero cells via ROS-dependent endoplasmic reticulum stress through PERK and IRE1 pathways. *Vet. Microbiol.* **2021**, *253*, 108959. [[CrossRef](#)]
33. Zafarullah, M.; Li, W.Q.; Sylvester, J.; Ahmad, M. Molecular mechanisms of N-acetylcysteine actions. *Cell. Mol. Life Sci. CMLS* **2003**, *60*, 6–20. [[CrossRef](#)]
34. Pilch, D.R.; Sedelnikova, O.A.; Redon, C.; Celeste, A.; Nussenzweig, A.; Bonner, W.M. Characteristics of γ -H2AX foci at DNA double-strand breaks sites. *Biochem. Cell Biol.* **2003**, *81*, 123–129. [[CrossRef](#)]
35. Solier, S.; Sordet, O.; Kohn, K.W.; Pommier, Y. Death Receptor-Induced Activation of the Chk2- and Histone H2AX-Associated DNA Damage Response Pathways. *Mol. Cell. Biol.* **2009**, *29*, 68–82. [[CrossRef](#)]
36. Solier, S.; Pommier, Y. The apoptotic ring: A novel entity with phosphorylated histones H2AX and H2B, and activated DNA damage response kinases. *Cell Cycle* **2009**, *8*, 1853–1859. [[CrossRef](#)]
37. Liu, X.; Zou, H.; Slaughter, C.; Wang, X. DFF, a Heterodimeric Protein That Functions Downstream of Caspase-3 to Trigger DNA Fragmentation during Apoptosis. *Cell* **1997**, *89*, 175–184. [[CrossRef](#)]
38. Song, J.H.; Shim, J.K.; Choi, H.J. Quercetin 7-rhamnoside reduces porcine epidemic diarrhea virus replication via independent pathway of viral induced reactive oxygen species. *Virol. J.* **2011**, *8*, 460. [[CrossRef](#)]
39. Rogakou, E.P.; Nieves-Neira, W.; Boon, C.; Pommier, Y.; Bonner, W.M. Initiation of DNA Fragmentation during Apoptosis Induces Phosphorylation of H2AX Histone at Serine 139. *J. Biol. Chem.* **2000**, *275*, 9390–9395. [[CrossRef](#)]
40. Smith, S.; Weller, S.K. HSV-I and the cellular DNA damage response. *Future Virol.* **2015**, *10*, 383–397. [[CrossRef](#)]
41. Full, F.; Ensser, A. Early Nuclear Events after Herpesviral Infection. *J. Clin. Med.* **2019**, *8*, 1408. [[CrossRef](#)]
42. Ren, S.; Ur Rehman, Z.; Gao, B.; Yang, Z.; Zhou, J.; Meng, C.; Song, C.; Nair, V.; Sun, Y.; Ding, C. ATM-mediated DNA double-strand break response facilitated oncolytic Newcastle disease virus replication and promoted syncytium formation in tumor cells. *PLoS Pathog.* **2020**, *16*, e1008514. [[CrossRef](#)] [[PubMed](#)]
43. Hammack, C.; Ogden, S.C.; Madden, J.C.; Medina, A.; Xu, C.; Phillips, E.; Son, Y.; Cone, A.; Giovinazzi, S.; Didier, R.A.; et al. Zika Virus Infection Induces DNA Damage Response in Human Neural Progenitors That Enhances Viral Replication. *J. Virol.* **2019**, *93*, e00638-19. [[CrossRef](#)] [[PubMed](#)]
44. Ledur, P.F.; Karmirian, K.; da Silva Gouveia Pedrosa, C.; Souza, L.R.Q.; Assis-de-Lemos, G.; Martins, T.M.; de Cassia Cavalheiro Gomes Ferreira, J.; de Azevedo Reis, G.F.; Silva, E.S.; Silva, D.; et al. Zika virus infection leads to mitochondrial failure, oxidative stress and DNA damage in human iPSC-derived astrocytes. *Sci. Rep.* **2020**, *10*, 1218. [[CrossRef](#)] [[PubMed](#)]
45. Zavadskis, S.; Weidinger, A.; Hanetseder, D.; Banerjee, A.; Schneider, C.; Wolbank, S.; Marolt Presen, D.; Kozlov, A.V. Effect of Diphenyleneiodonium Chloride on Intracellular Reactive Oxygen Species Metabolism with Emphasis on NADPH Oxidase and Mitochondria in Two Therapeutically Relevant Human Cell Types. *Pharmaceutics* **2021**, *13*, 10. [[CrossRef](#)] [[PubMed](#)]
46. Riganti, C.; Gazzano, E.; Polimeni, M.; Costamagna, C.; Bosia, A.; Ghigo, D. Diphenyleneiodonium Inhibits the Cell Redox Metabolism and Induces Oxidative Stress. *J. Biol. Chem.* **2004**, *279*, 47726–47731. [[CrossRef](#)]
47. Kučera, J.; Binó, L.; Štefková, K.; Jaroš, J.; Vašíček, O.; Večeřa, J.; Kubala, L.; Pacherník, J. Apocynin and Diphenyleneiodonium Induce Oxidative Stress and Modulate PI3K/Akt and MAPK/Erk Activity in Mouse Embryonic Stem Cells. *Oxidative Med. Cell. Longev.* **2016**, *2016*, 7409196. [[CrossRef](#)]
48. Li, N.; Ragheb, K.; Lawler, G.; Sturgis, J.; Rajwa, B.; Melendez, J.A.; Robinson, J.P. DPI induces mitochondrial superoxide-mediated apoptosis. *Free Radic. Biol. Med.* **2003**, *34*, 465–477. [[CrossRef](#)]
49. Longpre, J.M.; Loo, G. Paradoxical effect of diphenyleneiodonium in inducing DNA damage and apoptosis. *Free Radic. Res.* **2008**, *42*, 533–543. [[CrossRef](#)]

50. Cho, S.O.; Lim, J.W.; Kim, H. Diphenyleneiodonium Inhibits Apoptotic Cell Death of Gastric Epithelial Cells Infected with *Helicobacter pylori* in a Korean Isolate. *Yonsei Med. J.* **2015**, *56*, 1150–1154. [[CrossRef](#)]
51. Mah, L.J.; El-Osta, A.; Karagiannis, T.C. γ H2AX: A sensitive molecular marker of DNA damage and repair. *Leukemia* **2010**, *24*, 679–686. [[CrossRef](#)]
52. Rogakou, E.P.; Pilch, D.R.; Orr, A.H.; Ivanova, V.S.; Bonner, W.M. DNA Double-stranded Breaks Induce Histone H2AX Phosphorylation on Serine 139. *J. Biol. Chem.* **1998**, *273*, 5858–5868. [[CrossRef](#)]
53. Rodier, F.; Coppé, J.-P.; Patil, C.K.; Hoeijmakers, W.A.M.; Muñoz, D.P.; Raza, S.R.; Freund, A.; Campeau, E.; Davalos, A.R.; Campisi, J. Persistent DNA damage signalling triggers senescence-associated inflammatory cytokine secretion. *Nat. Cell Biol.* **2009**, *11*, 973–979. [[CrossRef](#)]
54. McManus, K.J.; Hendzel, M.J. ATM-dependent DNA damage-independent mitotic phosphorylation of H2AX in normally growing mammalian cells. *Mol. Biol. Cell* **2005**, *16*, 5013–5025. [[CrossRef](#)]
55. Andäng, M.; Hjerling-Leffler, J.; Moliner, A.; Lundgren, T.K.; Castelo-Branco, G.; Nanou, E.; Pozas, E.; Bryja, V.; Halliez, S.; Nishimaru, H.; et al. Histone H2AX-dependent GABAA receptor regulation of stem cell proliferation. *Nature* **2008**, *451*, 460–464. [[CrossRef](#)]
56. Barral, S.; Beltramo, R.; Salio, C.; Aimar, P.; Lossi, L.; Merighi, A. Phosphorylation of histone H2AX in the mouse brain from development to senescence. *Int. J. Mol. Sci.* **2014**, *15*, 1554–1573. [[CrossRef](#)]
57. de Feraudy, S.; Revet, I.; Bezrookove, V.; Feeney, L.; Cleaver, J.E. A minority of foci or pan-nuclear apoptotic staining of γ H2AX in the S phase after UV damage contain DNA double-strand breaks. *Proc. Natl. Acad. Sci. USA* **2010**, *107*, 6870–6875. [[CrossRef](#)]
58. Marti, T.M.; Hefner, E.; Feeney, L.; Natale, V.; Cleaver, J.E. H2AX phosphorylation within the G₁ phase after UV irradiation depends on nucleotide excision repair and not DNA double-strand breaks. *Proc. Natl. Acad. Sci. USA* **2006**, *103*, 9891–9896. [[CrossRef](#)]
59. Neelsen, K.J.; Zanini, I.M.Y.; Herrador, R.; Lopes, M. Oncogenes induce genotoxic stress by mitotic processing of unusual replication intermediates. *J. Cell Biol.* **2013**, *200*, 699–708. [[CrossRef](#)]
60. Ewald, B.; Sampath, D.; Plunkett, W. H2AX phosphorylation marks gemcitabine-induced stalled replication forks and their collapse upon S-phase checkpoint abrogation. *Mol. Cancer Ther.* **2007**, *6*, 1239–1248. [[CrossRef](#)]
61. Baure, J.; Izadi, A.; Suarez, V.; Giedzinski, E.; Cleaver, J.E.; Fike, J.R.; Limoli, C.L. Histone H2AX phosphorylation in response to changes in chromatin structure induced by altered osmolarity. *Mutagenesis* **2008**, *24*, 161–167. [[CrossRef](#)]
62. Meyer, B.; Voss, K.-O.; Tobias, F.; Jakob, B.; Durante, M.; Taucher-Scholz, G. Clustered DNA damage induces pan-nuclear H2AX phosphorylation mediated by ATM and DNA-PK. *Nucleic Acids Res.* **2013**, *41*, 6109–6118. [[CrossRef](#)]
63. Fragkos, M.; Breuleux, M.; Clément, N.; Beard, P. Recombinant Adeno-Associated Viral Vectors Are Deficient in Provoking a DNA Damage Response. *J. Virol.* **2008**, *82*, 7379–7387. [[CrossRef](#)]
64. Schwartz, R.A.; Carson, C.T.; Schuberth, C.; Weitzman, M.D. Adeno-Associated Virus Replication Induces a DNA Damage Response Coordinated by DNA-Dependent Protein Kinase. *J. Virol.* **2009**, *83*, 6269–6278. [[CrossRef](#)] [[PubMed](#)]
65. Zhang, Y.-j.; Lu, C.-r.; Cao, Y.; Luo, Y.; Bao, R.-f.; Yan, S.; Xue, M.; Zhu, F.; Wang, Z.; Duan, L.-n. Imatinib induces H2AX phosphorylation and apoptosis in chronic myelogenous leukemia cells in vitro via caspase-3/Mst1 pathway. *Acta Pharmacol. Sin.* **2012**, *33*, 551–557. [[CrossRef](#)] [[PubMed](#)]
66. Boege, Y.; Malehmir, M.; Healy, M.E.; Bettermann, K.; Lorentzen, A.; Vucur, M.; Ahuja, A.K.; Böhm, F.; Mertens, J.C.; Shimizu, Y.; et al. A Dual Role of Caspase-8 in Triggering and Sensing Proliferation-Associated DNA Damage, a Key Determinant of Liver Cancer Development. *Cancer Cell* **2017**, *32*, 342–359.e10. [[CrossRef](#)] [[PubMed](#)]